Journal of Biomedical Optics

SPIEDigitalLibrary.org/jbo

Tumor cell differentiation by label-free fluorescence microscopy

Petra Weber
Michael Wagner
Petra Kioschis
Waltraud Kessler
Herbert Schneckenburger

SPIE

Tumor cell differentiation by label-free fluorescence microscopy

Petra Weber,[a] Michael Wagner,[a] Petra Kioschis,[b] Waltraud Kessler,[c] and Herbert Schneckenburger[a]
[a]Hochschule Aalen, Institut für Angewandte Forschung, Beethovenstr. 1, 73430 Aalen, Germany
[b]Hochschule Mannheim, Institut für Molekular- und Zellbiologie, Paul-Wittsack-Strasse 10, 68163 Mannheim, Germany
[c]Steinbeis-Hochschule Berlin, Steinbeis-Institut Multivariate Datenanalyse, Herderstr. 47, 72762 Reutlingen, Germany

Abstract. Autofluorescence spectra, images, and decay kinetics of U251-MG glioblastoma cells prior and subsequent to activation of tumor suppressor genes are compared. While phase contrast images and fluorescence intensity patterns of tumor (control) cells and less malignant cells are similar, differences can be deduced from autofluorescence spectra and decay kinetics. In particular, upon near UV excitation, the fluorescence ratio of the free and protein-bound coenzyme nicotinamid adenine dinucleotide depends on the state of malignancy and reflects different cytoplasmic (including lysosomal) and mitochondrial contributions. While larger numbers of fluorescence spectra are evaluated by principal component analysis, a multivariate data analysis method, additional information on cell metabolism is obtained from spectral imaging and fluorescence lifetime imaging microscopy. [DOI: 10.1117/1.JBO.17.10.101508]

Keywords: glioblastoma cells; autofluorescence; nicotinamid adenine dinucleotide; spectral imaging; fluorescence lifetime imaging microscopy; multivariate data analysis.

Paper 12069SSP received Feb. 2, 2012; revised manuscript received Apr. 16, 2012; accepted for publication Apr. 23, 2012; published online Jun. 11, 2012.

1 Introduction

In label-free diagnostics of cells and tissues, intrinsic fluorescence and (nonelastic) light scattering appear to be promising methods. When excited by near ultraviolet light, autofluorescence of the coenzymes nicotinamid adenine dinucleotide (NADH; superposed by a small amount of phosphorylated NADPH) as well as flavin mono- and dinucleotide (FMN/FAD) seems to play a predominant role, since it reflects their state of oxidation and, consequently, cell physiology.[1–3] Therefore, autofluorescence measurements have been used to study states of hypoxia,[4] oxidative stress in neurodegenerative diseases,[5] or mitochondrial malfunction.[6] In addition, based on different cell metabolism and tissue properties, autofluorescence was used increasingly for tumor detection of various organs including bladder, lung, larynx, breast, or skin.[7–13] However, a comparison of tumor cells and less malignant cells was revealed to be difficult, so far, due to the lack of comparable cell lines. In the present paper this difficulty was circumvented by use of so-called isogenic cells prior and subsequent to activation of tumor suppressor genes.

Fluorescence spectra, images, and decay times, including spectral as well as fluorescence lifetime images (FLIM), are presently compared, and principal component analysis (PCA), a multivariate statistical method,[14–16] is used to evaluate complex data sets. Part of the cells was incubated either with the lysosomal marker Lysotracker Yellow (LY) or the mitochondrial marker Mitotracker Orange (MO), since these dyes proved to be helpful for intracellular localization of autofluorescence. All experiments were carried out under strict control of light dose upon irradiation in order to maintain cell viability. Phase contrast images were used for comparative studies of cell morphology.

2 Materials and Methods

Experiments described in this paper were carried out with genetically engineered U251-MG glioblastoma cells kindly supplied by Prof. Jan Mollenhauer, Department of Molecular Oncology, University of South Denmark, Odense. In two subclones of those U251 cells, the tumor suppressor genes TP53 or PTEN were overexpressed using a Tet-On inducible expression system (with doxycycline), such that these cells exhibited a reduced tumorigenic potential and may be regarded as less malignant. Highly malignant U251-MG cells without suppressor gene (part of which was also incubated with doxycycline) were used as controls. Cells were seeded at a density of 150 mm^{-2} and cultivated for 72 h at 37 °C and 5% CO_2 as monolayers on glass slides in medium DMEM supplemented with 10% FCS and hygromycin B. Part of the cells was incubated either with Lysotracker Yellow (LY; 75 nM; 45 min.) or Mitotracker Orange (MO; 25 nM; 30 min.) diluted in culture medium.

A wide-field microscope (Axioplan 1, Carl Zeiss Jena, Germany) was equipped with a 375-nm picosecond laser diode (LDH 375 with driver PDL 800-B, PicoQuant, Berlin, Germany; pulse energy: 12 pJ, pulse duration: 55 ps, repetition rate: 40 MHz) for fluorescence excitation. An irradiance of 100 mW/cm^2 or less permitted measuring times up to 250 s under strict maintenance of cell viability.[17] Fluorescence images were recorded with a 63 × /0.90 water immersion objective lens and an electron multiplying (EM-)CCD camera (DV887DC, ANDOR Technology, Belfast, U.K.) with Peltier cooling and a sensitivity below 10^{-16} W/pixel. This EM-CCD camera was replaced by an image intensifying camera system (Picostar HR 12 image intensifier coupled to a cooled CCD camera; LaVision,

Address all correspondence to: Herbert Schneckenburger, Hochschule Aalen, Institut für Angewandte Forschung, Beethovenstr. 1, 73430 Aalen, Germany. Tel: +49 7361 576 3401; Fax: +49 7361 576 3318; E-mail: herbert.schneckenburger@htw-aalen.de

0091-3286/2012/$25.00 © 2012 SPIE

Göttingen, Germany), which was triggered by the laser diode, for fluorescence lifetime measurements at a resolution of 200 ps. Decay kinetics of whole single cells were fitted by two exponential components, while fluorescence images recorded within successive 200 ps time gates were evaluated by a monoexponential fitting algorithm for FLIM.

Fluorescence spectra of single cells were recorded with a custom made polychromator and an image intensifying detection unit (IMD 4562, Hamamatsu Photonics, Ichino-Cho, Japan) at a resolution of 10 nm. A commercial program (Unscrambler 9.8; Camo Process AS, Oslo, Norway) was used for PCA. This statistical method reduces multidimensional data into few principal components, which constitute a new, lower-dimensional coordinate system for describing the fluorescence spectra. Common information (which is found by explaining as much of the variable variation as possible with the lower-dimensional coordinate system) is summarized in the principal components (PC). The impact of each individual spectral variable on a PC is expressed in the loadings spectra. The spectra themselves are described by their score values in the new PC coordinate system. Thus no reference spectra of individual components are needed a priori for evaluation of the fluorescence data set.

For spectral imaging the polychromator was replaced by interference filters for 450 ± 20 nm and 490 ± 20 nm located in front of the EM-CCD camera (s. above), so that images in these spectral ranges could be measured selectively and further evaluated, as described below.

3 Results

In Fig. 1, fluorescence spectra of U251-MG glioblastoma cells (malignant controls as well as less malignant cells with suppressor genes TP53 or PTEN activated by doxycycline) are depicted. All spectra are dominated by broad bands with maxima around 440 to 450 nm and 470 to 490 nm, which have previously been attributed to protein-bound and free NADH, respectively, as well as by a long-wave shoulder around 530 nm assigned to flavins.[1,2] Obviously, the long-wave NADH band is more prominent for the malignant controls than for the less malignant cells. This effect was further evaluated by PCA. After normalization of all spectra the first, second, and third principal components (PC1, PC2, PC3), which describe 97% of the total spectral variation, were calculated. Since PC3 reveals major differences between tumor (control) cells and less malignant cell lines, its loadings and scores are depicted in Fig. 2. Obviously, the loadings of PC3 [Fig. 2(a)] reveal main differences between the cell lines in the wavelength range of 430 to 460 nm, which is the range of bound NADH. The scores plot in Fig. 2(b) quantifies all the fluorescence spectra related to PC3. Most of the PC3 scores show positive values for the control cells (independent from whether they were incubated with doxycycline or not) and negative values for cells with activated suppressor genes TP53 or PTEN (by doxycycline). Positive score values [Fig. 2(b)] combined with positive loading values [Fig. 2(a)] imply that fluorescence intensities of the controls (tumor cells) were higher in the range of $\lambda = 460$ to 530 nm, whereas positive score values [Fig. 2(b)] combined with negative loadings [Fig. 2(a)] indicate that fluorescence intensities of the controls were lower at 430 to 460 nm in comparison with the less malignant cells. This proves that the ratio of free/bound NADH was higher in the tumor cells than in the less malignant cells. When fluorescence images were measured selectively at 450 ± 20 nm (I_{450}) and 490 ± 20 nm (I_{490}), the ratio PBP $= (I_{450} - I_{490})/(I_{450} + I_{490})$ reflected the relation of bound/free NADH and was therefore assigned "protein binding parameter." This parameter is depicted in Fig. 3 (left column) and shows particularly low values in fluorescent granules surrounding the cell nucleus.

Fluorescence decay kinetics of all cell lines after excitation by picosecond laser pulses showed a bi-exponential behavior according to $I(t) = A_1 e^{-t/\tau 1} + A_2 e^{-t/\tau 2}$ with $\tau_1 = 0.4$ to 0.5 ns and $\tau_2 = 2.3$ to 2.8 ns, similar to data reported earlier for free NADH and protein-bound NADH, respectively.[18,19] In comparison with the control cells, τ_2 slightly increased for

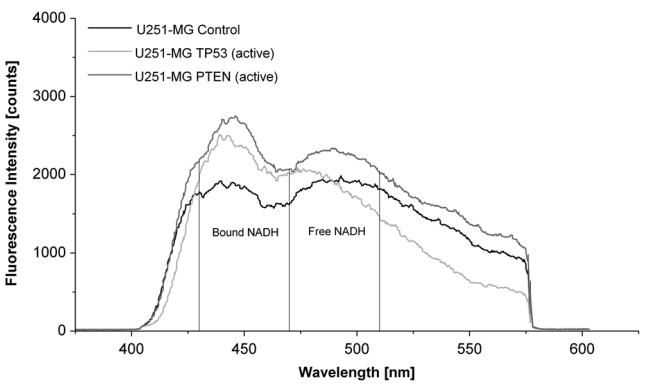

Fig. 1 Autofluorescence spectra of a U251-MG glioblastoma cell (control) and cells with activated suppressor genes TP53 or PTEN (excitation wavelength: 375 nm; detection range: 400 to 580 nm). Intervals used for spectral imaging are indicated.

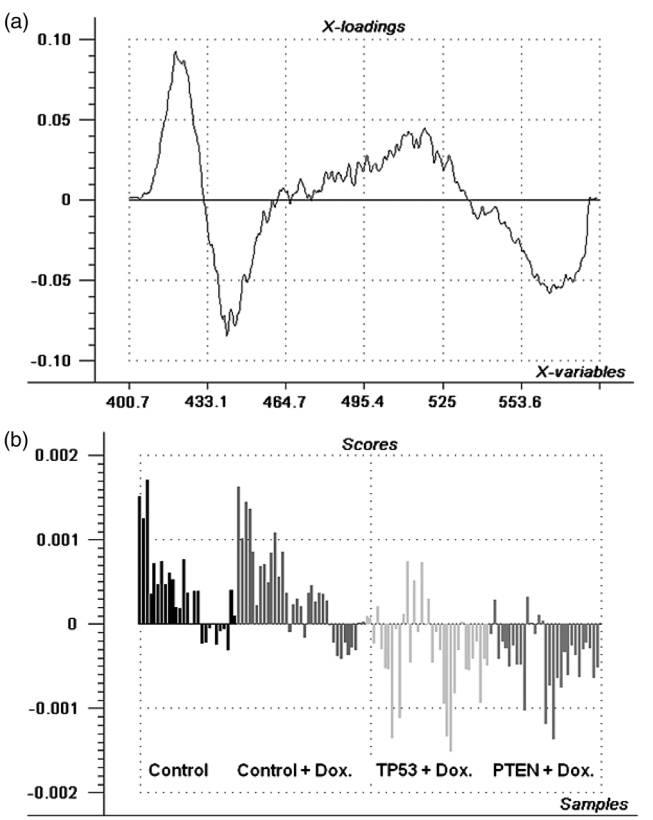

Fig. 2 Evaluation of autofluorescence spectra by principal component analysis (PCA); (a) loadings and (b) scores of PC3 for a set of about 140 individual spectra of U251-MG control cells and cells with activated suppressor genes TP53 or PTEN.

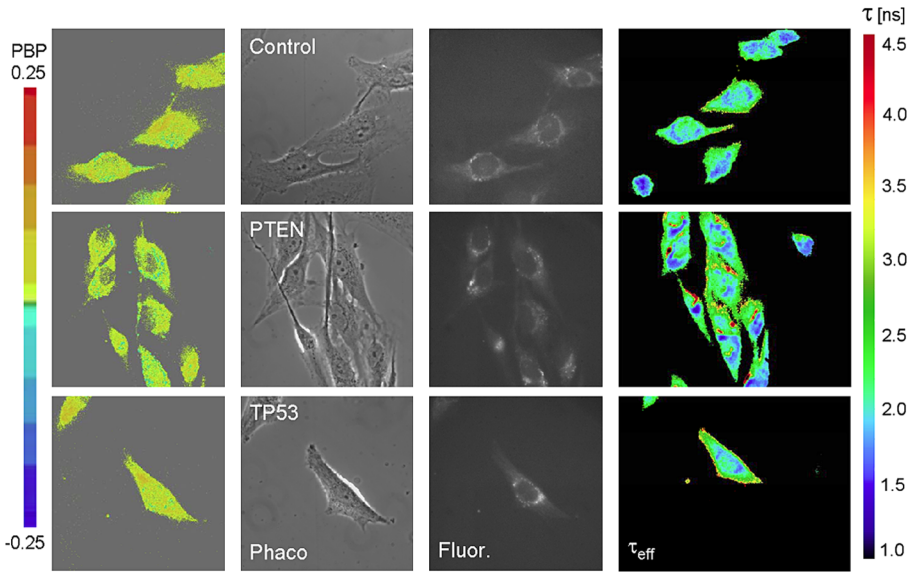

Fig. 3 Protein binding parameter (PBP), phase contrast images, fluorescence intensity, and effective fluorescence lifetime τ_{eff} (from left to right) of U251-MG control cells and cells with activated suppressor genes TP53 or PTEN.

the less malignant cells from 2.3 ± 0.2 ns to 2.7 to 2.8 ns, as determined in each case from 30 individual measurements of control cells as well as from cells with activated tumor suppressor genes TP53 and PTEN. This indicates slight changes in the contribution or intracellular interaction of protein-bound NADH. In Fig. 3, phase contrast, fluorescence intensity, PBP, and fluorescence lifetime images of U251-MG control cells and cells with activated suppressor genes TP53 or PTEN are compared. Instead of individual fluorescence lifetimes τ_1 and τ_2, the so-called effective fluorescence lifetime τ_{eff} resulting from monoexponential curve fitting (and depending on both NADH species) is depicted in the right column. This lifetime is generally reduced from 2.0 to 2.2 ns to values around 1.6 ns in the fluorescent granules surrounding the cell nucleus. Outside these granules τ_{eff} appears slightly longer in the cells with activated suppressor genes PTEN and TP53 as compared with the controls.

In addition to the fluorescent granules surrounding the cell nucleus, some long-shaped rods appear in the fluorescence intensity patterns of all cell types (third column of Fig. 3). In a first step to identify fluorescent organelles, part of the cells was incubated either with LY or MO. In Fig. 4, patterns of autofluorescence (excited at 375 nm and detected by an interference filter at 450 to 490 nm) are compared with LY fluorescence (excited by a mercury high pressure lamp at 450 to 490 nm and detected at wavelengths above 520 nm). While fluorescent granules around the cell nucleus appear to be the same in both images, the long-shaped rods as well as some diffuse fluorescence from other parts of the cytoplasm are missing in the LY image. In contrast, these rods become obvious after incubation with MO (excited by the same mercury lamp at 510 to 560 nm and detected at wavelengths above 590 nm; Fig. 5). Therefore, in addition to lysosomes, mitochondria appear to be main sources of autofluorescence, as also reported in the literature (for a review see Ref. 3).

4 Discussion

The principal purpose of this study was to identify parameters by which tumor cells and less malignant cells of the same genetic background can be distinguished. An appropriate parameter seems to be the ratio of protein-bound versus free NADH, also described in this paper as protein binding parameter (PBP). Further information can be obtained from fluorescence lifetimes of NADH. Here, differences between individual cell lines are small, but some information is deduced from fluorescence lifetime images, which identify fluorescent granules surrounding the cell nucleus as organelles with lowest effective fluorescence lifetimes. Autofluorescence of these granules coincides with the fluorescence pattern of the lysosomal marker LY, suggesting that these granules might represent lysosomes, small vacuoles or

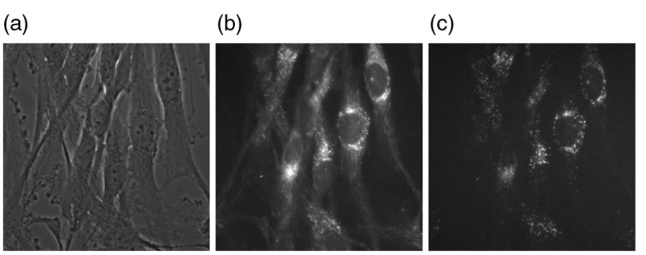

Fig. 4 U251-MG glioblastoma cells (controls) incubated with Lysotracker Yellow (LY); (a) phase contrast; (b) autofluorescence (λ_{ex} = 375 nm; λ_d = 450 to 490 nm); (c) LY fluorescence (λ_{ex} = 450 to 490 nm; $\lambda_d \geq 520$ nm); image size: 140 × 140 µm.

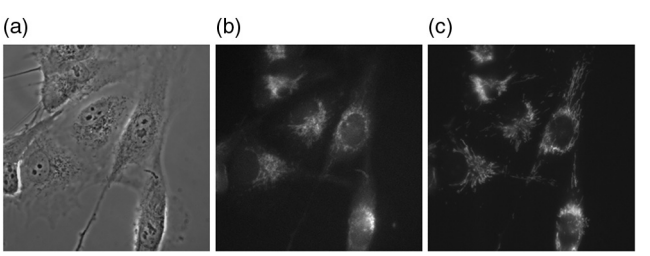

Fig. 5 U251-MG glioblastoma cells (controls) incubated with Mitotracker Orange (MO); (a) phase contrast; (b) autofluorescence (λ_{ex} = 375 nm; λ_d = 450 to 490 nm); (c) MO fluorescence (λ_{ex} = 510 nm to 560 nm; $\lambda_d \geq 590$ nm); image size: 140 × 140 µm.

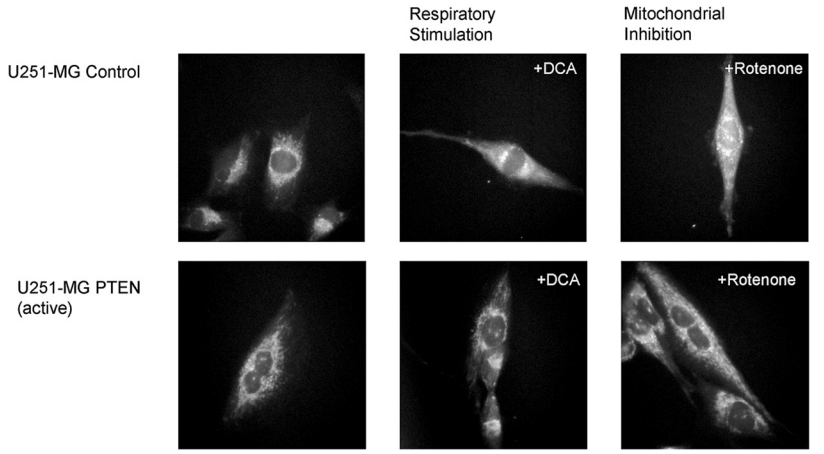

Fig. 6 U251-MG glioblatoma cells (controls and cells with an activated suppressor gene PTEN) prior and subsequent to respiratory stimulation by dichloracetate (DCA) or mitochondrial inhibition by rotenone (excitation wavelength: ($\lambda_{ex} = 375$ nm; detection range: $\lambda_d \geq 420$ nm; image size: 140×140 μm).

related organelles. Also in the literature[20] lysosomes have been described as a main source of autofluorescence, with some major contribution of the age pigment lipofuscin. Since both, emission wavelength and fluorescence lifetime of lipofuscin overlap with that of free NADH, the nature of autofluorescence in the granules requires further investigation. Mitochondrial fluorescence also seems to play a predominant role in autofluorescence measurements. When respiration of the cells was stimulated by dichloracetate (DCA), mitochondrial fluorescence increased considerably in the tumor (control) cells, but remained almost constant in the cells with activated tumor suppressor genes, as is visualized in Fig. 6 for control cells and cells with the activated tumor suppressor gene PTEN. This indicates some metabolic change within the tumor cells upon stimulation, possibly some shift from anaerobic glycolysis to respiration, in agreement with earlier findings.[3] In Fig. 6 also, the effect of inhibition of the respiratory chain by rotenone is depicted. This figure shows some fluorescence increase (partly originating from the long shaped rods representing mitochondria) for both cell lines, similar to earlier findings of BKEz-7 endothelial cells.[21] Only future experiments may prove whether this fluorescence increase is affected by activation of tumor suppressor genes. In summary, differences in autofluorescence properties between tumor cells and less malignant cells seem to reflect their different cell metabolism and may be used for diagnostic purposes. Possibly, quantitative assessment of flavin fluorescence or FAD/NADH ratios[22] might further improve tumor cell discrimination.

For a reliable distinction, however, further parameters, e.g., cell growth or cell age, as well as cell adhesion to a substrate[23] should be considered. In addition, other types of cancer cells should be examined by similar methods. For example, MCF-7 breast cancer cells transfected either with the proliferation inhibitor and apoptosis regulator p21 or with the pro-oncogene c-myc showed only minor differences of fluorescence spectra and lifetimes in comparison with MCF-7 control cells (results not shown). Finally, in tissue further fluorescent components, resulting e.g., from extracellular collagen or elastic fibers,[7,24,25] as well as an inhomogeneous illumination, resulting in variations of fluorescence intensity, should be taken into account. Due to all these uncertainties it is suggested to combine autofluorescence measurements with other label-free methods, e.g., Raman scattering.[26–28] Preliminary Raman experiments[29] exhibited slight differences between U251-MG control cells and cells with activated suppressor genes, mainly originating from granules surrounding the cell nucleus. However, only future experiments will prove whether these differences can be quantified reliably.

For all studies of cell metabolism, it is indispensable to maintain the cells' viability and function. In particular, phototoxic properties of NADH[30] and flavins[31] should be taken into account, and damage by high light exposure should be avoided. As previously reported,[17] a light dose of 25 J/cm^2 (corresponding to 0.25 μJ/μm^2) at an excitation wavelength of 375 nm or 100 J/cm^2 (corresponding to 1 μJ/μm^2) at 514 nm may be regarded as a maximum for maintaining cell viability. This dose corresponds to 250 to 1000 s of solar illumination and may be easily exceeded in 3-D microscopy.[17,32] Therefore, in fluorescence or Raman microscopy low irradiance has to be combined with highly sensitive detection units, e.g., EM-CCD cameras, image intensifying systems, or very sensitive spectroscopic devices.

Acknowledgments

We would like to thank the Bundesministerium für Bildung und Forschung (BMBF) for funding our research in grant no. 17 92C 08 and Baden-Württemberg-Stiftung gGmbH for financing project "Aurami." We also thank Dr. Rainer Wittig (ILM Ulm) for stimulating discussions. Cooperation with Dr. Hella Kuhn (Hochschule Mannheim) and technical assistance by Claudia Hintze (Hochschule Aalen) are gratefully acknowledged.

References

1. T. Galeotti et al., "On the fluorescence of NAD(P)H in whole cell preparations of tumors and normal tissues," *Eur. J. Biochem.* **17**, 485–496 (1970).
2. J.-M. Salmon et al., "Microspectrofluorometric approach to the study of free/bound NAD(P)H ratio as metabolic indicator in various cell types," *Photochem. Photobiol.* **36**, 4585–4593 (1982).
3. A. A. Heikal, "Intracellular coenzymes as natural biomarkers for metabolic activities and mitochondrial anomalities," *Biomarkers Med.* **4**(2), 241–263 (2010).
4. E. T. Obi-Tabot et al., "Changes in hepatocyte NADH fluorescence during prolonged hypoxia," *J. Surg. Res.* **55**(6), 575–580 (1993).

5. N. Braidy, G. Guillemin, and R. Grant, "Promotion of cellular NAD(+) anabolism: therapeutic potential for oxidative stress in ageing and Alzheimer's disease," *Neurotox. Res.* **13**(3–4), 173–184 (2008).
6. M. H. Gschwend et al., "Optical detection of mitochondrial NADH content in human myotubes," *Cell. Mol. Biol.* **47**, OL95–OL104 (2001).
7. S. Andersson-Engels et al., "Fluorescence imaging and point measurements of tissue: applications to the demarcation of malignant tumors and atherosclerotic lesions from normal tissue," *Photochem. Photobiol.* **53**(6), 807–814 (1991).
8. J. Hung et al., "Autofluorescence of normal and malignant bronchial tissue," *Lasers Surg. Med.* **11**(2), 99–105 (1991).
9. B. Banerjee et al., "Emission spectra of colonic tissue and endogenous fluorophores," *Am. J. Med. Sci.* **316**(3), 220–226 (1998).
10. M. A. D'Hallewin et al., "Fluorescence detection of bladder cancer: a review," *Eur. Urol.* **42**(5), 417–425 (2002).
11. D. C. de Veld et al., "The status of in vivo autofluorescence spectroscopy and imaging for oral oncology," *Oral Oncol.* **41**(2), 117–131 (2005).
12. M. Monici, "Cell and tissue autofluorescence research and diagnostic applications," *Biotechnol. Annu. Rev.* **11**, 227–256 (2005).
13. T. Gabrecht et al., "Optimized autofluorescence bronchoscopy using additional backscattered red light," *J. Biomed. Opt.* **12**(6), 064016 (2007).
14. C. Eker et al., "Multivariate analysis of laryngeal fluorescence spectra recorded in vivo," *Lasers Surg. Med.* **28**(3), 259–266 (2001).
15. J. Y. Qu et al., "Fluorescence spectral imaging for characterization of tissue based on multivariate spectral analysis," *J. Opt. Soc. Am. A* **19**(9), 1823–1831 (2002).
16. D. M. Haaland et al., "Hyperspectral confocal fluorescence imaging: exploring alternative multivariate curve resolution approaches," *Appl. Spectrosc.* **63**(3), 271–279 (2009).
17. M. Wagner et al., "Light dose is a limiting factor to maintain cell viability in fluorescence microscopy and single molecule detection," *Int. J. Mol. Sci.* **11**, 956–966 (2010).
18. H. Schneckenburger and K. König, "Fluorescence decay kinetics and imaging of NAD(P)H and flavinsas metabolic indicators," *Opt. Eng.* **31**(7), 1447–1451 (1992).
19. Q. Yu and A. H. Heikal, "Two-photon autofluorescence dynamics imaging reveals sensitivity of intracellular NADH concentration and conformation to cell physiology at the single cell level," *J. Photochem. Photobiol. B:Biol.* **95**(4), 47–56 (2009).
20. H. Andersson et al., "Autofluorescence of living cells," *J. Microsc.* **191**, 1–7 (1998).
21. H. Schneckenburger et al., "Energy transfer spectroscopy for measuring mitochondrial metabolism in living cells," *Photochem. Photobiol.* **66**(1), 33–41 (1997).
22. J. H. Ostrander et al., "Optical redox ratio differentiates breast cancer cells based on estrogen receptor status," *Cancer Res.* **70**(11), 4759–4766 (2010).
23. M. Wagner, P. Weber, and H. Schneckenburger, "Nanotomography of cell adhesion upon variable-angle Total Internal Reflection Fluorescence Microscopy (VA-TIRFM)," *J. Vis. Exp.*, in press (2012).
24. J. Siegel et al., "Studying biological tissue with fluorescence lifetime imaging: microscopy, endoscopy, and complex decay profiles," *Appl. Opt.* **42**(16), 2995–3003 (2003).
25. R. Orzekowsky-Schroeder et al., "In vivo spectral imaging of different cell types in the small intestine by two-photon excited autofluorescence," *J. Biomed. Opt.* **16**(11), 116025 (2011).
26. I. F. Nabiev, H. Morjani, and M. Manfait, "Selective analysis of antitumor drug interaction with living cells as probed by surface-enhanced Raman spectroscopy," *Eur. Biophys. J.* **19**(6), 311–316 (1991).
27. K. Chen et al., "Diagnosis of colorectal cancer using Raman spectroscopy of laser-trapped single living epithelial cells," *Opt. Lett.* **31**(13), 2015–2017 (2006).
28. C. M. Krishna et al., "Raman spectroscopy of breast tissues," *Expert Rev. Mol. Diagn.* **8**(2), 149–166 (2008).
29. H. Schneckenburger et al.,"Tumor cell differentiation by marker free fluorescence microscopy," *Proc. SPIE* **7902**, 79020D (2011).
30. L. M. Tiede and M. G. Nichols, "Photobleaching of reduced nicotinamide adenine dinucleotide and the development of highly fluorescent lesions in rat basophilic leukaemia cells during multiphoton microscopy," *Photochem. Photobiol.* **82**(3), 656–664 (2006).
31. P. Hockberger et al., "Activation of flavin-containing oxidases underlies light-induced production of H_2O_2 in mammalian cells," *Proc. Natl. Sci. U.S.A.* **96**(11), 6255–6260 (1999).
32. H. Schneckenburger et al., "Light exposure and cell viability in fluorescence microscopy," *J. Microsc.* **245**(3), 311–318 (2012).